

Modeling the Flight Dynamics and Battery Utilization of a Hybrid Flapping-Gliding UAV

Lena Johnson*, Derek A. Paley[†], and Hugh A. Bruck[‡]
University of Maryland, College Park, MD 20742

This paper presents a hybrid flapping-gliding dynamic model for a flapping-wing unmanned aerial vehicle (UAV). The model combines the nonlinear phugoid dynamics of gliding flight, the equations of motion of the onboard servo motors, and an equivalent circuit discharge model for the onboard battery. The resulting state-space representation relates the aerodynamic flight performance to onboard energy utilization: the battery life is expended when the UAV flaps and is preserved when the UAV glides. Flapping flight is described by the phugoid model augmented to include thrust. An equivalent circuit model describes the onboard lithium-polymer battery discharge behavior and resulting input into the platform's servo motor actuators. The model is illustrated via numerical simulations using parameter values based on the RoboRaven experimental testbed. Performance of intermittent gliding-flapping behavior is evaluated in terms of battery longevity and overall distance travelled.

I. Nomenclature

x	=	Horizontal position
z	=	Vertical position
θ	=	Flight path angle
v	=	Flight speed
Ω	=	Motor angular rate
I_{mot}	=	Motor current
Z_{bat}	=	Battery state-of-charge
V_{bat}	=	Battery voltage
R_{bat}	=	Battery discharge resistance
I_{bat}	=	Battery current
Q_{bat}	=	Battery capacity
C_D	=	Coefficient of drag
$C_{L,glide}$	=	Gliding coefficient of lift
$C_{L,flap}$	=	Flapping coefficient of lift
C_T	=	Coefficient of thrust
K_I	=	Motor torque coefficient
b	=	Motor damping coefficient
J	=	Motor moment of inertia
R_{mot}	=	Motor coil resistance
L	=	Motor inductance
K_{emf}	=	Electromotive force constant
K_g	=	Gear ratio
K_{SOC}	=	State-of-charge constant

*PhD candidate, Department of Mechanical Engineering

[†]Willis H. Young Jr. Professor of Aerospace Engineering Education, Department of Aerospace Engineering and Institute for Systems Research and AIAA Senior Member

[‡]Professor, Department of Mechanical Engineering, and Associate Dean for Faculty Affairs, A. James Clark School of Engineering

II. Introduction

NOVEL applications for Unmanned Aerial Vehicle (UAV) technologies are constantly expanding. UAVs are increasingly being used in missions involving the management of resources or the preservation of human life, such as agricultural monitoring and search and rescue missions. Many applications require more reliable and longer flights—often in unstructured, dynamic environments. However, current UAV flight time is limited by onboard battery capacity and weight. Though battery technology itself is progressing with increased capacity and lower weight, it remains a challenge to ensure that the UAV is capable of achieving sufficient flight time.

Methods to address extending UAV flight time typically fall into one of two categories. The first category focuses on improving battery chemistry, battery capacity, or system integration [1–3]. However, this approach is limited by current battery-chemical technology and the addition of weight due to heavier components. The second methodology increases flight efficiency by advantageously using atmospheric phenomena via energy-harvesting techniques. These methods, which include static and dynamic soaring and intermittent gliding, are often bio-inspired [4–6]. Soaring and gliding improve flight time and extend onboard battery life without requiring additional weight or battery capacity. Furthermore, gliding is useful even in atmospheric conditions that lack features favorable for energy harvesting.

Flapping-wing UAVs have been developed for a variety of purposes, and an increasing number of them are able to perform prolonged, untethered flight in dynamic environments. Examples include Delfly [7, 8], Batbot [9], and Robird [10]. There are even insect-inspired varieties such as RoboBee [11] and a robotic dragonfly [12]. RoboRaven is a servo-driven flapping-wing UAV with independent wing control capable of prolonged, outdoor flights [1, 2, 13–15].

This paper presents a hybrid state-space model of a UAV capable of gliding and flapping. The contributions are (1) inclusion of thrust in the classical phugoid model of flight dynamics to represent a flapping vehicle; (2) combining the flight-dynamics model with the equations of motion of the onboard motors and the battery discharge dynamics to describe the overall system in state-space form; and (3) numerical evaluation of intermittent flapping-gliding behavior using the quantitative performance metrics of battery endurance and flight distance. Ultimately, this modeling framework will support the experimental demonstration of intermittent gliding techniques on the RoboRaven flapping-wing UAV.

The paper is organized as follows. Section III provides an overview of the phugoid model of a gliding vehicle, the battery discharge model, and the RoboRaven experimental testbed. Section IV presents the state-space model combining flight, motor, and battery dynamics and provides numerical illustrations. Section V quantifies performance as a function of the gliding-to-flapping duty cycle. Section VI summarizes the paper and ongoing work.

III. Background

This section describes the phugoid model of flight dynamics, battery modeling via equivalent circuit theory, and the RoboRaven flapping-wing UAV.

A. Phugoid Model of a Gliding Vehicle

Phugoid theory [16] is a mathematical representation of aircraft gliding and stall behavior. Phugoid dynamics arise from examining the aircraft equations of motion in the longitudinal plane. Utilizing these dynamics makes it possible to quantify and predict the flight path of an aircraft. Following [17], we derive a state-space representation based on the forward flight speed and flight path angle of the aircraft.

Consider a point-mass model of an aircraft where θ is the flight path angle and the aircraft velocity is $v\hat{b}_1$ (see Figure 1). Applying Newton’s second law yields

$$-mg\hat{e}_2 - F_{drag}\hat{b}_1 + F_{lift}\hat{b}_2 = m(\dot{v}\hat{b}_1 + v\dot{\theta}\hat{b}_2). \quad (1)$$

Separating (1) into \hat{b}_1 and \hat{b}_2 components yields

$$m\dot{v} = -mg \sin \theta - F_{drag} \quad (2)$$

$$mv\dot{\theta} = -mg \cos \theta + F_{lift}. \quad (3)$$

Assuming quadratic models for the forces of lift and drag, the state-space equations of motion are

$$\dot{v} = -g \sin \theta - C_D v^2 \quad (4)$$

$$\dot{\theta} = \frac{-g \cos \theta + C_{L,glide} v^2}{v}, \quad (5)$$

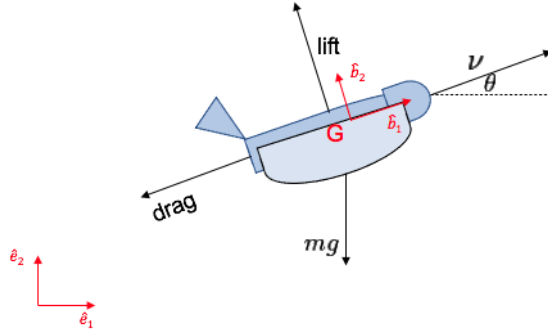


Fig. 1 The forces and coordinates of the phugoid dynamics, after [17]

where C_D and C_{Lglide} are the coefficients of drag and lift while gliding, respectively. These equations are augmented with thrust to describe the flapping mode of flight in Section IV.

B. Battery Dynamic Modeling

Modeling a battery's charging and discharging behavior is a complex process that depends on which aspects of the battery are most relevant to the application. An equivalent circuit model describes battery behavior using elements of electric circuits. Such models vary in complexity and accuracy and are, therefore, widely applicable for modeling systems that regard the battery as an integral component.

Figure 2 illustrates an idealized model of battery discharge behavior that uses a Thévenin equivalent circuit with resistance R_{bat} to describe the internal battery resistance during discharge [18]. Let V_{bat} denote the battery discharge

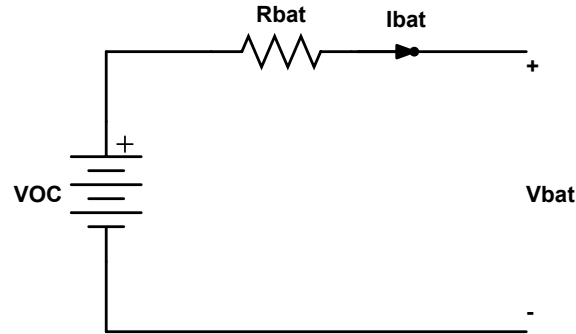


Fig. 2 The equivalent circuit model for battery discharge [18]

voltage and I_{bat} the discharge current. Applying Kirchoff's law to the circuit yields

$$V_{bat} = VOC - R_{bat} I_{bat}, \quad (6)$$

where VOC represents the open circuit voltage.

When modeling simple batteries, VOC is approximately equal to the battery's state of charge (SOC). However, when modeling more complex battery systems, the relationship between VOC and SOC might be nonlinear [19, 20], e.g., polynomial or exponential [21, 22]. SOC tracks the remaining charge in the battery in order to describe the amount of power being supplied and is often represented as a percentage of the fully charged state. There exist a variety of methods by which a battery's SOC is tracked. One of the most widely used is the Coulomb counting method [15, 23, 24], in which SOC is represented as the integral of the time-varying current $I_{bat}(t)$ over the battery's capacity Q_{bat} , i.e.,

$$SOC(t) = SOC(0) - \int_0^t \frac{I_{bat}(\tau)}{Q_{bat}} d\tau. \quad (7)$$

There are many methods by which an equivalent circuit model can be refined to describe more complex battery systems more accurately. One method of increasing the model’s complexity is to increase the order of the Thévenin circuit by adding RC circuit elements to capture the long-term and short-term transient behavior inherent in lithium batteries during discharge [21]. In the following section, we improve model accuracy by varying the battery resistance R_{bat} as an exponential function of SOC [15, 21] in order to capture the relationship between the battery’s discharge behavior and the internal resistance’s decay curve.

C. RoboRaven Experimental Testbed

RoboRaven is a servo-driven flapping-wing UAV with independent wing control capable of prolonged, outdoor flight [1, 2, 13–15]. This platform, developed in collaboration between researchers at the University of Maryland and the University of Southern California, is an adaptable and controllable aerial vehicle. The original RoboRaven design has been extended to accommodate larger wing sizes [13], autonomous flight [14], solar-energy capture [2], and flexible battery integration [1]. Prior work on system modeling of the onboard servos and lipo-batteries [15] developed governing equations using a Thévenin equivalent and run-time circuit method [21]. Experimental data was used to fit and validate the equivalent circuit model and servo components with low error.



Fig. 3 RoboRaven is a flapping wing UAV developed at the University of Maryland [25].

RoboRaven is also capable of operating as a mixed-mode flapping-wing UAV [25], using the addition of rear propellers to increase payload capacity and maneuverability. The addition of propellers also enables the platform to reach even higher altitudes and speeds. (The study of propeller-aided flight is outside the scope of this paper and is the subject of ongoing and future analysis.) Instead we assume the thrust is generated solely by wing flapping and, therefore, scales with the square of flapping frequency [25]. Flapping-wing UAVs are uniquely suited to improve flight longevity through periodic gliding as described next.

IV. Hybrid Gliding-Flapping Dynamics

This section combines the state-space model of the phugoid dynamics, the battery discharge model during the flapping phase, and the corresponding motor dynamics to describe onboard energy utilization during intermittent flapping-gliding behavior. Two state-space models were used, one that describes the platform’s gliding behavior using the phugoid model (4–5) and another that adapts the phugoid model to describe flapping behavior. For the flapping mode, the lift coefficient is decreased as compared to gliding. In addition, the phugoid model (4–5) is augmented to include thrust generated during the flapping mode [25]. Thrust is proportional to the square of the wing-flapping frequency, which is related to the motor angular rate of rotation by the gear ratio K_g . Let C_T denote the coefficient of thrust. During flapping flight, (4) becomes

$$\dot{v} = -g \sin \theta - C_D v^2 + \frac{C_T}{K_g^2} \Omega^2. \quad (8)$$

Assume the onboard servos are a common electro-mechanical motor whose dynamics are described by a resistor-inductor circuit with backwards electromotive force (EMF). Back EMF relates the motor’s angular velocity to the

internal current. Let K_I denote the motor torque coefficient, b the motor damping coefficient, J the motor moment of inertia, and the last term denotes the load torque. The dynamics of the motor angular rate arise from Euler's second law, i.e.,

$$\dot{\Omega} = \frac{K_I}{J} I_{mot} - \frac{b}{K_g^2 J} \Omega - \frac{1}{J} \Omega. \quad (9)$$

The corresponding dynamics for the motor current from Kirchoff's law are

$$\dot{I}_{mot} = \frac{1}{L} V_{bat} - \frac{R_{mot}}{L} I_{mot} - \frac{K_{emf}}{L} \Omega \quad (10)$$

where R_{mot} is the motor coil resistance, L the motor inductance, and K_{emf} the electromotive force constant. Finally, because the direction of current in the motor coils is the opposite of the direction in the battery, let $I_{bat} = -I_{mot}$.

The onboard lithium-polymer battery is modeled by differentiating the equivalent circuit model (6) and the Coulomb counting model (7) with respect to time, assuming $R_{bat} = R_{bat}(t)$ and $VOC = SOC = Z_{bat} \in [0, 1]$ are state variables. Following [18, 21], R_{bat} is an exponential function of Z_{bat} given by

$$R_{bat} = R_{bat}(0)(1 - e^{K_{SOC} Z_{bat}}), \quad (11)$$

which implies

$$\dot{R}_{bat} = -R_{bat}(0) K_{SOC} e^{K_{SOC} Z_{bat}} \dot{Z}_{bat}. \quad (12)$$

Figure 4 illustrates the effect of the parameter $K_{SOC} < 0$ on the battery discharge behavior, where $R_{bat}(0) = 0.036$.

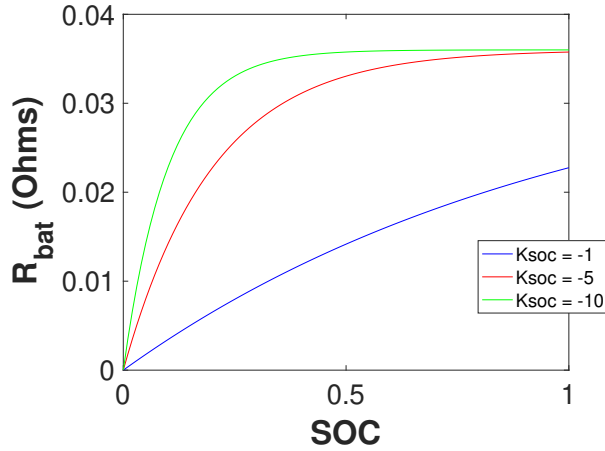


Fig. 4 The effect of K_{SOC} on the battery resistance R_{bat}

The equations of motion combining the flight, motor, and battery dynamics during the flapping phase are

$$\dot{x} = v \cos \theta \quad (13)$$

$$\dot{z} = v \sin \theta \quad (14)$$

$$\dot{\theta} = \frac{-g \cos \theta + C_{L,flap} v^2}{v} \quad (15)$$

$$\dot{v} = -g \sin \theta - C_D v^2 + \frac{C_T}{K_g^2} \Omega^2 \quad (16)$$

$$\dot{\Omega} = \frac{K_I}{J} I_{mot} - \frac{b}{K_g^2 J} \Omega - \frac{1}{J} \Omega \quad (17)$$

$$\dot{I}_{mot} = \frac{1}{L} V_{bat} - \frac{R_{mot}}{L} I_{mot} - \frac{K_{emf}}{L} \Omega = -\dot{I}_{bat} \quad (18)$$

$$\dot{Z}_{bat} = -\frac{I_{bat}}{Q_{bat}} \quad (19)$$

$$\dot{R}_{bat} = -R_{bat}(0) K_{SOC} e^{K_{SOC} Z_{bat}} \dot{Z}_{bat} \quad (20)$$

$$\dot{V}_{bat} = \dot{Z}_{bat} - R_{bat} \dot{I}_{bat} - \dot{R}_{bat} I_{bat} \quad (21)$$

When the platform is gliding, the battery and motor dynamics are disengaged and the state-space equations revert to the original phugoid model (4-5). Tables 1 and 2 list the model variables and parameters, respectively. Some parameters, such as the battery's initial resistance $R_{bat}(0)$ and the gear ratio K_g , were determined experimentally.

State	Description	Units	Initial Value
x	Horizontal position	m	0
z	Vertical position	m	2
θ	Flight path angle	rad	0
v	Flight speed	m/sec	7.4
Ω	Motor angular rate	rad/sec	0
I_{mot}	Motor current	A	1
Z_{bat}	Battery SOC	N/A	1
R_{bat}	Battery internal resistance	ohms	0.036
V_{bat}	Battery voltage	V	8.5

Table 1 State variables of the combined flight, motor, and battery dynamical system

Figure 5 depicts a numerical simulation of the state-space system (13–21) for the flapping mode using initial conditions and parameters in Table 1 and 2. The battery discharged over time as the servos consume energy. The flight path is parabolic, because the vehicle gained altitude only when the motor angular rate was sufficiently high. As the battery voltage dropped, the motor angular rate decreased and the vehicle descended even while flapping. Z_{bat} was normalized to fit in the range [0,1]. The impact of implementing an intermittent gliding duty cycle on battery longevity and flight endurance is examined next.

V. Glide Cycle Design and Performance Analysis

Natural flyers utilize a variety of intermittent flight modalities based upon constraints such as atmospheric conditions, energy level, and altitude. This section describes simulations that test the effects of intermittent flapping on flight longevity. To evaluate the performance of intermittent gliding and flapping, we considered battery endurance and the effective flight distance. Even though the shut-off voltage of the RoboRaven battery is 5V [15], the vehicle gains altitude while flapping only when the battery voltage exceeds 6V. Therefore, battery endurance was defined as the duration of time the battery provides 6V or more. Furthermore, the platform should maintain a minimum height during flight. The effective flight distance is the horizontal distance traveled while remaining higher than the initial altitude.

Parameter	Description	Units	Value
C_D	Coefficient of drag	N/A	0.1–0.5
$C_{L,flap}$	Coefficient of lift during flapping	N/A	0.5–1
$C_{L,glide}$	Coefficient of lift during gliding	N/A	1–2
C_T	Coefficient of thrust	N/A	386.4
g	gravity	m/sec ²	9.81
K_{emf}	Electromotive force constant	V/rad/sec	0.4
b	Motor damping coefficient	N·m·sec	0.5–0.2
K_g	Gear ratio	N/A	169.87
J	Moment of inertia	kg·m ²	0.01
L	Motor inductance	H	0.01
R_{mot}	Motor coil resistance	Ohms	0.5–0.2
K_I	Motor torque coefficient	N·m/A	1.63
R_{init}	Battery discharge resistance	Ohms	0.036
Q_{bat}	Battery capacity	A·sec	1332
K_{SOC}	Resistance parameter	N/A	-(2–5)

Table 2 Parameters of the combined flight, motor, and battery dynamical system

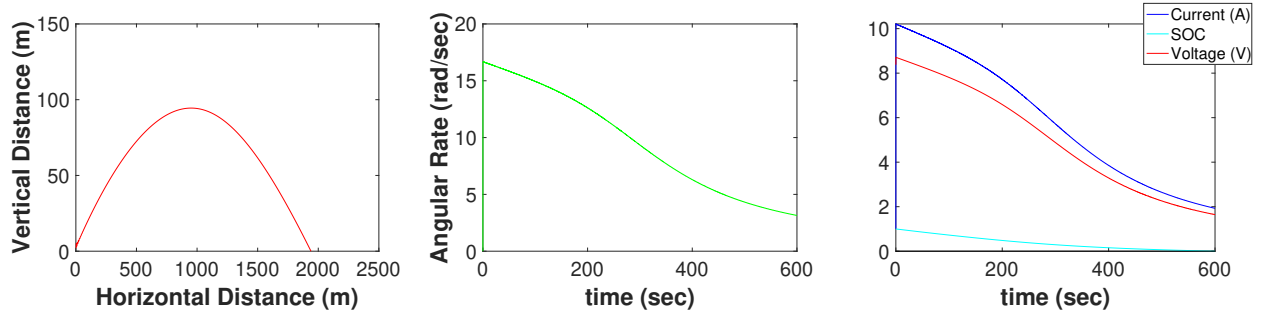


Fig. 5 Model simulation in flapping mode: (a) longitudinal dynamics; (b) angular rate and flight speed; and (c) onboard energy usage.

The intermittent flapping modality is characterized by the amount of time the platform stays in the flapping or gliding stages, i.e., the duty cycle. The duty cycle can be symmetric, i.e., time spent flapping or gliding is the same, or asymmetric. Both symmetric and asymmetric duty cycles were tested to determine their respective effects on the model. Duty cycles were measured in seconds as shown in Table 3.

The simulation results indicate a universal increase in battery endurance and flight distance when intermittent gliding is used. Figure 6 shows a 10-second symmetric duty cycle simulation, and Figure 7 shows the longitudinal dynamics for a chosen series of duty cycles. Furthermore, the tabulated results shown in Figure 8 show that duty cycles with longer periods of gliding (both asymmetric and symmetric) yield the most improvement in the performance metrics compared to the nominal case of all flapping. Specifically, the two asymmetric duty cycles with the longest gliding and shortest flapping times (30-10 and 20-10) performed the best in improving the performance metrics.

VI. Conclusion

This paper presents a state-space model describing intermittent flapping and gliding behavior of a flapping wing unmanned aerial vehicle by combining the phugoid model of flight dynamics, an electro-mechanical motor model, and a Thévenin equivalent battery model. The state-space representation directly relates the gliding-flapping performance of

Duty Cycles (glide - flap)
10 - 10
20 - 20
30 - 30
10 - 20
10 - 30
20 - 10
30 - 10

Table 3 Duty cycles for the simulated experiments (seconds)

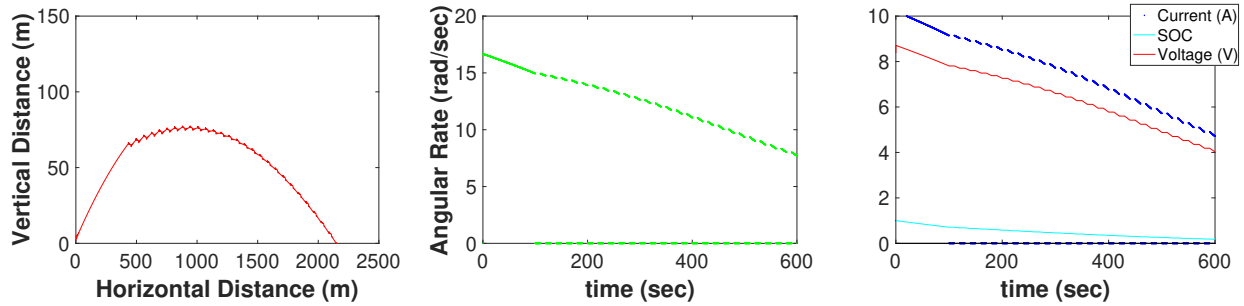


Fig. 6 Model simulation with a 10-10 second duty cycle: (a) longitudinal dynamics; (b) angular rate and flight speed; and (c) onboard energy usage.

the platform to the onboard energy utilization. Numerical simulations show that all of the chosen intermittent glide cycles increased the battery endurance and flight distance. In ongoing and future work, the model will be revised to include propeller-driven flight and higher fidelity battery dynamics. The numerical model will also be validated experimentally via a test stand and outdoor flight tests using the RoboRaven platform.

References

- [1] Holness A. E., Solheim H., Bruck H. A., and Gupta S. K., "A Design Framework for Realizing Multifunctional Wings for Flapping Wing Air Vehicles Using Solar Cells," *International Journal of Micro Air Vehicles*, Vol. 11, No. 1, 2019, pp. 1–19.
- [2] Perez-Rosado, A., "Design, fabrication, and Characterization of Multifunctional Wings to Harvest Solar Energy in Flapping Wing Air Vehicles," Ph.D. thesis, University of Maryland - College Park, 2015.
- [3] Donato T., Ficarella A., Spedicato L., Arista A., and Ferraro M., "A New Approach to Calculating Endurance in Electric Flight and Comparing Fuel Cells and Batteries," *Applied Energy*, Vol. 187, No. 1, 2017, pp. 807–819.
- [4] Depenbusch N., Bird J., and Langelaan J., "The AutoSOAR Autonomous Soaring Aircraft Part 2 Hardware Implementation and Flight Results," *Journal of Field Robotics*, Vol. 35, No. 4, 2017, pp. 435–458.
- [5] Stolle M., Wanatabe Y., Doll C., and Bolting J., "Vision-Based Lifespan and Strength Estimation of Sub-Cumulus Thermal Updrafts for Autonomous Soaring," In Proceedings of the International Conference on Unmanned Aircraft Systems, 2016.
- [6] Bird J., and Langelaan J., "Design Space Exploration for Hybrid Solar/Soaring Aircraft," In Proceedings of the AIAA Aviation Technology, Integration, and Operations Conference, 2017.
- [7] Caetano J. V., Percin M., DeVisser C., VanOudheusden B., DeCroon G. C. H. E., DeWatger C., Remes B., and Mulder M., "Tethered vs. Free Flight Force Determination of the DelFly II Flapping Wing Micro Air Vehicle," In Proceeding of the International Conference on Unmanned Aircraft Systems, 2014.
- [8] De Croon G. C. H. E. , Groen M. A., Wagter C. D., Remes B., Ruijsink R., and Oudheusden, B. W. V. , "Design, Aerodynamics and Autonomy of the DelFly," *Bioinspiration & Biomimetics*, Vol. 7, No. 2, 2012, pp. 1–36.

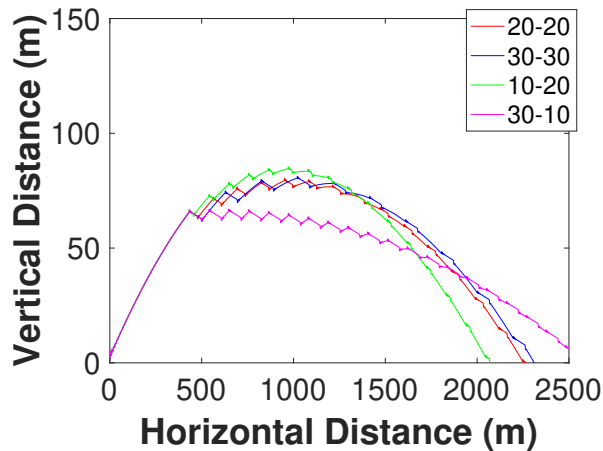


Fig. 7 Model simulation of the longitudinal dynamics with varied gliding duty cycles (see Table 3)

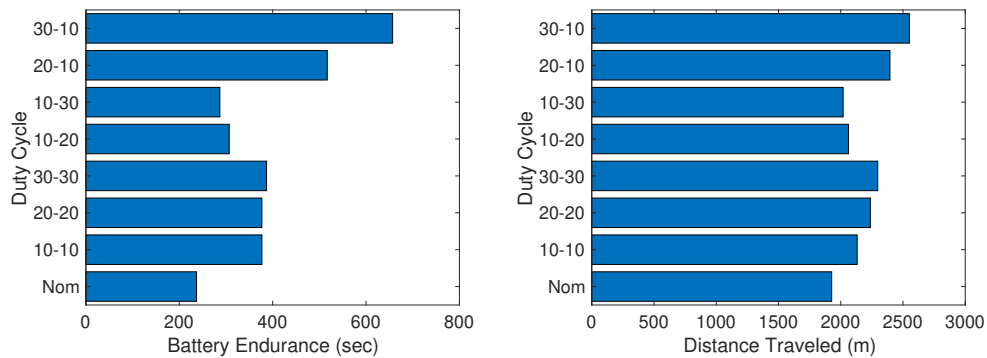


Fig. 8 Simulation results for gliding: (a) battery endurance vs. glide cycle; (b) flight distance vs. glide cycle

[9] Ramezani A., Chung S. J., and Hutchinson S., "A Biomimetic Robotic Platform to Study Flight Specializations of Bats," *Science Robotics*, Vol. 2, 2017, p. 2505.

[10] Folkertsma G. A., Straatman W., Nijenhuis N., Venner C. H., and Stramigioli S., "Robird: A Robotic Bird of Prey," *IEEE Robotics & Automation*, Vol. 24, No. 3, 2017, pp. 22–29.

[11] Finio B., and Wood R., "Open-Loop Roll, Pitch, Yaw Torques for a Robotic Bee," In Proceedings of the International Conference on Intelligent Systems and Robotics, 2012.

[12] Gaissert N., Mugrauer R., Mugrauer G., Jebens A., and Jebens K., "Inventing a Micro Aerial Vehicle Inspired by the Mechanics of Dragonfly Flight," In Proceedings of Towards Autonomous Robotic Systems. TAROS 2013. Lecture Notes in Computer Science, 2014, pp. 90–100.

[13] Gerdes J., Bruck H., and Gupta S. K., "A Systematic Exploration of Wing Size on Flapping Wing air Vehicle Performance," In Proceeding of ASME IDETC/CIE, 2015.

[14] Roberts L. J., Bruck H. A., and Gupta S. K., "Modeling of Dive Maneuvers for Executing Autonomous Dives With a Flapping Wing Air Vehicle," *Journal of Mechanisms and Robotics*, Vol. 9, No. 6, 2017, pp. 1–16.

[15] Gerdes, J., "Improved Prediction of Flapping Wing Aerial Vehicle Performance Through Component Interaction Modeling," Ph.D. thesis, University of Maryland - College Park, 2018.

[16] Lanchester F. W., *Aerodnetics: Constituting the Second Volume of a Complete Work on Aerial Flight*, London: A. Constable, London, 1908.

- [17] Sunderland, S., *The Art of Phugoid*, 2020 (accessed: 06.08.2020). URL http://www.math.stonybrook.edu/~scott/Book331/Art_Phugoid.html.
- [18] Saldana, G., and San Martin, J.I., and Zamora, I., and Asensio, F. J., and Onederra, O., “Analysis of the Current Electric Battery Models for Electric Vehicle Simulation,” *Energies*, Vol. 12, No. 14, 2019, pp. 2750–2777. <https://doi.org/10.3390/en12142750>.
- [19] Zhang, R., Xia, B., Li, B., Cao, L., Lai, Y., Zheng, W., Weng, H., Wang, W., and Wang, M., “A Study on the Open Circuit Voltage and State of Charge Characterization of High Capacity Lithium-Ion Battery Under Different Temperature,” *Energies*, Vol. 11, No. 9, 2018, pp. 2408–2425. <https://doi.org/10.3390/en11092408>.
- [20] Zhang, C., Jiang, J., Zhang, L., Liu, S., Wang, L., and Loh, P. C., “A Generalized SOC-OCV Model for Lithium-Ion Batteries and the SOC Estimation for LNMCO Battery,” *Energies*, Vol. 9, No. 11, 2016, pp. 900–916. <https://doi.org/10.3390/en9110900>.
- [21] Chen, M., and Rincon-Mora, G. A., “Accurate Electrical Battery Model Capable of Predicting Run-time and I-V Performance,” *IEEE Transactions on Energy Conversion*, Vol. 21, No. 2, 2006, pp. 504–511.
- [22] Hinz, H., “Comparison of Lithium-Ion Battery Models for Simulating Storage Systems in Distributed Power Generation,” *Inventions*, Vol. 4, No. 3, 2019, pp. 41–63. <https://doi.org/10.3390/inventions4030041>.
- [23] Chang, W., “The State of Charge Estimating Methods for Battery: A Review,” *ISRN Applied Mathematics*, Vol. 2013, No. 1-7, 2013. <https://doi.org/10.1155/2013/953792>.
- [24] Vergori, E., Mocera, F., and Soma, A., “Battery Modeling and Simulation Using a Programmable Testing Equipment,” *Computers*, Vol. 7, No. 20, 2018, pp. 162–167. <https://doi.org/10.3390/computers7020020>.
- [25] Holness, A., Bruck, H., and Gupta, S. K., “Characterizing and Modeling the Enhancement of Lift and Payload Capacity Resulting from Thrust Augmentation in a Propeller-Assisted Flapping Wing Air Vehicle,” *International Journal of Micro Air Vehicles*, Vol. 10, No. 1, 2017, pp. 50–69.